Object-Based Cognitive Map in the Human Hippocampus and Medial Prefrontal Cortex

Authors: Bo Zhang[1] and Yuji Naya[1, 2, 3, 4, 5, *]

Affiliations:

[1] School of Psychological and Cognitive Sciences, Peking University, No. 52, Haidian Road, Haidian District, Beijing 100805, China

[2] Center for Life Sciences, Peking University, No. 52, Haidian Road, Haidian District, Beijing 100805, China

[3] IDG/McGovern Institute for Brain Research at Peking University, No. 52, Haidian Road, Haidian District, Beijing 100805, China

[4] Beijing Key Laboratory of Behavior and Mental Health, Peking University, No. 52, Haidian Road, Haidian District, Beijing 100805, China

[5] Lead contact

Contact Info: *Correspondence: yujin@pku.edu.cn

Summary

A cognitive map, representing an environment around oneself, is necessary for spatial navigation. However, compared with its constituent elements such as individual landmarks, neural substrates of the coherent spatial information remain largely unknown. The present study investigated how the brain codes map-like representations in a virtual environment specified by relative positions of three objects. Representational similarity analysis revealed the object-based spatial environment in the hippocampus (HPC) when participants located their self-positions within it, while the medial prefrontal cortex (mPFC) represented it when they recollected a target object's location relative to their self-body. During the recollection, task-dependent functional connectivity increased between the two areas implying exchange of self- and target-location signals between HPC and mPFC. Together, the coherent cognitive map may be recruited in HPC and mPFC for complementary functions when we relate ourselves with a target object including person for navigation, and presumably for social interactions.

Key words: cognitive map, spatial navigation, episodic memory, memory-guided decision making, social interaction, hippocampus, medial prefrontal cortex, default mode network, representational similarity analysis.

Introduction

During navigation, it is necessary to locate our self-position in the current spatial environment as well as to locate the objects relative to the self-body (i.e., egocentric location). To conduct each of the two mental operations, we need map-like representations, called "cognitive map" in our brain (Tolman, 1948). After the discovery of "place cells," the hippocampus (HPC) of the medial temporal lobe (MTL) has been considered responsible for the cognitive map (Buffalo, 2015), and crucial contributions of the HPC to spatial memory have also been reported by animal model studies that evaluated behavioral patterns of rodents with an inactivated HPC using the Morris water maze and cross-maze (Nakazawa et al., 2002; Packard and McGaugh, 1996; Redish and Touretzky, 1998) as well as human studies that demonstrated the relationship between HPC volume in individual subjects and their amounts of experience exploring spatial environments (Woollett and Maguire, 2011; Schinazi et al., 2013, e.g., London taxi drivers). However, it remains largely unknown how neural substrates of the cognitive map are involved in the two mental operations required for the recollection of an egocentric location of a target object. One possible reason for the difficulty in addressing this question is that despite extensive studies on the spatial elements related to the cognitive map (e.g., self-location, head-direction etc.) (O'Keefe and Dostrovsky, 1971; Vass and Epstein, 2013; Chadwick et al., 2015; Buffalo, 2015; McCormick et al., 2018;), there is still a lack of sufficient isolation and characterization of the neural signal of the cognitive map under the previous research paradigms.

In addition to the HPC, the role of the medial prefrontal cortex (mPFC) in goal-directed planning during navigation was demonstrated by a previous human fMRI study that showed increased connectivity between the HPC and mPFC (Brown et al., 2016). The mPFC has been long considered as a member of the core-brain system in the retrieval of episodic memory (Konishi et al., 2000; Eichenbaum, 2017; McCormick et al., 2018), which is an

autobiographical memory consisting of spatial, object, and temporal information (Suzuki and Naya, 2011; Naya and Suzuki, 2011; Squire and Wixted, 2011). Schacter et al. (2007) suggested an involvement of the mPFC in future-simulation processing and recollection of past episodes, which depend on mnemonic information stored as declarative memory including both episodic and semantic memory. Recently, they also showed increased connectivity between the HPC and mPFC during future simulation (Campbell et al., 2018). This preceding literature suggests that the HPC and mPFC, which belong to the default-mode network, work together when remembering stored information (e.g., cognitive map) and construct the mental representation of goal-directed information (e.g., target-location) from mnemonic information with the current context (e.g., self-location) (Schacter, 2012). However, the specific functional role of each of HPC and mPFC during the construction process (McCormick et al., 2018; Campbell et al., 2018) remain elusive, presumably because the construction of goal-directed information (e.g., spatial navigation) includes at least two mental operations described above (i.e., locating self and locating the target relative to self-location), and the previous experimental paradigms mostly unseparated them.

To address these issues, we aimed to devise a novel 3D spatial-memory task with spatial environments defined by objects, which would enable us to identify the representation of the cognitive map and to investigate how it is related to the two mental operations (Fig. 1). We used the same stimulus set consisting of three different human characters through the entire experiment, while the spatial configuration of the three characters was changed trial-by-trial. The spatial configuration pattern was referred to as a *"map"* in the present study (Fig. 1b). In each trial, participants encoded a *map* from the first-person's view by walking toward the characters in one of four fixed walking directions (walking period, Fig. 1c, see Methods). Following the walking period, one human character (facing object) was presented on a virtual-environment background with other characters being invisible**,** which gave the

86 participants a feeling of facing the presented character in the virtual environment (i.e., facing
87 period). After a short delay, one of the two remaining characters (targeting object) was
88 presented without the virtual environment background, and the participants were required to
89 remember the location of this second human character relative to their self-body (i.e.,
90 targeting period). Thus, the two mental operations were separated into two periods within a
91 single trial. This task design allowed us to detect the brain regions that distinguished the
92 spatial configurations of the objects (i.e., *map*) around the participants during the facing
93 period and targeting period separately. The results of the representational similarity analysis
94 (RSA; see Methods for details) (Kriegeskorte et al., 2012; Kriegeskorte et al., 2008) showed
95 that the spatial environment defined by the three objects were represented in the HPC during
96 the facing period, while it was represented in the vmPFC during the targeting period,
97 suggesting different contributions of the object-based cognitive map to the recollection
98 between the two brain areas of the default mode network.

Results

The experiment was conducted in two days with 19 participants. On the first day, the participants were familiarized with the 3D virtual environment and the three human characters through a head-nodding detection (HND) task (Fig. S1a). In this task, the participants had the same walking experience as in the spatial-memory task but were subsequently asked to indicate whether a character in a photo nodded its head during the walking period. On the second day, the participants performed the spatial-memory task under scanning. To prevent voluntary memorization of the spatial relationship of the human characters during the walking period, the HND trials were pseudo-randomly mixed with the spatial-memory trials at the ratio of 1:10, and the participants were instructed to focus on head-nodding of the human characters during the walking period in all trials. All participants exhibited a top-ceiling performance with a 93.6% ± 0.02% correct rate (mean ± SE, n = 19) for the spatial-memory task and no significant difference was found among each of the task parameters (e.g., maps, walking directions) (Fig. S1c). All participants showed an accuracy that was significantly higher than chance level (50%) in both the head-nodding and no head-nodding trials (Fig. S1a). Attempts to memorize the spatial arrangements of the human characters during scanning were examined using post-scanning questionnaires. All participants reported that they did not make any voluntary effort to memorize the spatial relationship of the three human characters nor utilize any special strategy for memorizing it (Table S2). It should be noted that no participant was able to recall the number of map patterns they experienced in the experiment even though only three of the six possible patterns of maps were repeatedly presented to each participant. In addition, no significant changes in performance was found across four experimental sessions (Fig. S1b; $F(3,72) = 0.38$, $P < 0.001$), suggesting that the participants performed the spatial-memory task with high-performance from the beginning and did not learn to use a systematic strategy to

improve their performance during the sessions. These behavioral results guarantee that the participants automatically encoded maps during the walking period when viewing the human characters attentively to detect head-nodding.

Neural representation of the cognitive map during locating self-position

We first assessed the map representation during the facing period (4.0 s including the subsequent delay; Fig. 2a), in which the participants oriented themselves to a presented human character in the 3D environment. To decode the map information across the whole brain, we conducted searchlight-based RSA, which compared the multi-voxel pattern similarities of the "same map" and "different map" between trial pairs across each brain voxel by drawing a 6 mm radius sphere with each voxel in the spherical center. Map information was decoded regardless of other task parameters such as the walking direction or the identity of the facing character (see Methods for details and Table S1 for the regressor list and the averaged r^2 among the regressors in each GLM). We found a cluster located in the left middle HPC (mHPC; Fig. 2b, $P < 0.01$, voxel-wise threshold; $P < 0.05$, cluster-corrected), suggesting that the map defined by multiple objects is represented in the HPC. In addition to the mHPC, the searchlight-based RSA revealed clusters in the insula, angular gyrus, and superior temporal cortex (Fig. S2b, $P < 0.01$, voxel-wise threshold; $P < 0.05$, cluster-corrected; see discussion). To validate the searchlight-based RSA result showing that the left mHPC represents map information, we manually segmented the sub-regions in the MTL in each participant's native space (Fig. S4, left panel) and conducted an independent RSA within each anatomical mask (see Methods for details). The region of interest (ROI)-based result also showed that only the left mHPC had a significantly higher pattern similarity to "same maps" relative to "different maps" among the MTL sub-regions (Fig. S5a; $t(18) = 2.94$, $P = 0.004$, Bonferroni corrected for multiple comparisons, alpha < 0.05).

To examine possible signal input from the MTL sub-regions to the left mHPC for the map construction, we examined the neural representation of the facing-character identity and walking direction that the participants perceptually and/or mentally re-experienced during the facing period based on the post-scanning test (Table S2; Fig. S3a). Searchlight-based RSA revealed that the bilateral perirhinal cortex (PRC) encoded character identity (Fig. S3b; $P < 0.001$, initial threshold; $P < 0.05$, cluster-corrected) (Naya et al., 2001; Suzuki and Naya, 2014), while the parahippocampal cortex (PHC) and left retrosplenial cortex (RSC) encoded the walking directions reflecting the spatial layout of one empty and three occupied positions perceived by the participants during the walking period (Fig. 1c). In the HPC, the left posterior HPC (pHPC) selectively represented the spatial layout but not the character identity, while the bilateral anterior HPC (aHPC) revealed clusters for both character identity and spatial layout (Fig. S3b). These results were consistent with the notion of the "two cortical systems" model that suggests that object identity and spatiotemporal context are processed in two separate neural systems with the PRC and PHC-RSC as the core brain regions, with the two different information domains interacting in the HPC (Ranganath and Ritchey., 2012). Together, the RSA analyses demonstrated that the MTL is crucial for representing the spatial environment in the following ways**:** elements such as each object identity and spatial layout were represented by extrahippocampal areas while the relative relationship between multi-objects was represented in the HPC, suggesting cognitive map representation in the HPC.

Cognitive map during localizing target

In contrast to locate self-position, a clear difference was found in brain regions responsible for the map representations when the participants remembered the location of a target character relative to their self-body (egocentric target location). In contrast to the facing period, clusters representing the map information were revealed mainly in the Rectus and

174 Brodmann area 10 of the vmPFC (Peak coordinates: 4, 50, -18; t value: 5.62), rather than in
175 the HPC, during the targeting period. We confirmed that no cluster was found in the MTL
176 even though a more liberal threshold was used ($P < 0.01$, voxel-wise threshold, uncorrected).
177 To validate this result, we conducted an independent RSA using frontal sub-regions of the
178 automated anatomical labeling (AAL, Fig. S4, right panel) template as well as manually
179 segmented MTL sub-regions as ROIs. The result confirmed that the map information was
180 represented in the rectus of the prefrontal region (Fig. S5a, $t(18) = 4.64$, $P = 0.0001$,
181 Bonferroni corrected for multiple comparisons, alpha < 0.05), while no MTL sub-regions
182 revealed map representation significantly during the targeting period. Together with the
183 facing period results, these results revealed a double dissociation of MTL and mPFC function
184 in the map representation between the task demands, implying that the mPFC, rather than the
185 MTL, carried the map information during the generation of the egocentric location signal of a
186 target character but during self-body locating. Our results indicate that the HPC and mPFC
187 operate in a complementary manner, supporting the notion of the "parallel, but interactive
188 cognitive map" between the two brain structures (Wikenheiser and Schoenbaum., 2016).
189 Outside of the vmPFC, we found clusters in the precuneus and middle temporal gyrus, and
190 the inferior frontal cortex (Fig. 2c, Fig. S2c; $P < 0.001$, voxel-wise threshold; $P < 0.05$,
191 cluster-corrected). These three brain regions have been consistently reported to be involved in
192 scene construction during recalling of past experience and imagination of new experiences
193 (Hassabis and Maguire, 2007; Bird et al., 2010; Gaesser et al., 2013), which is consistent with
194 the post-scanning report showing that all participants recalled and also imagined the
195 egocentric positions of the three human characters during the targeting period.
196 As with the facing period, we examined neural representation of targeting character
197 identity and walking direction during the targeting period and found that the PRC stably
198 represented character identity (Fig. S3b; $P < 0.001$, initial threshold; $P < 0.05$, cluster-

corrected), while we did not find clusters for the spatial layout depending on the walking direction. These results suggested that the HPC did not construct the map information from its constituent elements during the targeting period.

Current self-orientation on the map

To compute the egocentric location of a target object (e.g., left, right, or back), information on the current self-position/orientation on the map is necessary (Fig. 3a). Therefore, we examined which brain regions were involved in representing such allocentric "heading-direction" signals (Hargreaves et al., 2005; Wang et al., 2018). Interestingly, while no significant cluster was revealed during the facing period (facing character; Fig. 3b and Supplementary Fig. S5b), robust clusters were revealed during the targeting period (Fig. 3b, $P < 0.001$, voxel-wise threshold; $P < 0.05$, cluster-corrected). These clusters were located in the ERC, bilateral HPC, and PHC inside the MTL as well as in the lateral occipital cortex, parietal cortex, precuneus, and anterior cingulate cortex outside the MTL (Fig. 3b, $P < 0.001$, voxel-wise threshold; $P < 0.05$, cluster-corrected). These results suggested that a self-orientation signal was induced during the targeting period, presumably because of the necessity to compute the egocentric target location. This interpretation is consistent with the post-scanning report in which participants reported imagining their self-orientation on the map only during the targeting period.

To further evaluate the role of the MTL in informational representation, we conducted a ROI-based RSA that computed the averaged pattern similarity among MTL sub-regions for four spatial parameters (cognitive map, walking direction, character identity, and self-orientation). The result revealed that the map and walking direction were represented in the MTL during the facing period (Fig. 3c, cognitive map: $t(18) = 2.519$, $P = 0.01$; walking direction: $t(18) = 5.134$, $P = 3.48$ x 10-5) followed by an attenuated-representation during the

targeting period (cognitive map: $t(18) = 1.312$, $P = 0.1$; walking direction: $t(18) = 2.302$, $P = 0.02$); in contrast, self-orientation was represented in the targeting period only (facing period: $t(18) = -2.256$, $P = 0.98$; targeting period: $t(18) = 7.11$, $P = 6.28 \times 10^{-7}$); Notably, the MTL showed significant representation for character identity in each period (facing period: $t(18) = 7.732$, $P = 1.98 \times 10^{-7}$; targeting period: $t(18) = 6.687$, $P = 1.42 \times 10^{-6}$). These results demonstrated that MTL encoded or reinstated the information of an external world around the participants which were necessary for determining an egocentric target location.

Remembering the egocentric location of a target object

Next, we examined which brain regions signaled the egocentric location (left, right, or back relative to self-body) of a target object (Fig. 4a). The results revealed robust clusters in both the mPFC and MTL (Fig. 4a, $P < 0.001$, voxel-wise threshold; $P < 0.05$, cluster-corrected). In the mPFC, we identified the rectus, medial/superior orbitofrontal cortex, and olfactory cortex. In the MTL, clusters were found in the anterior HPC. Apart from the mPFC and MTL, clusters were also found in the lateral occipital cortex, inferior parietal cortex, anterior temporal lobe, premotor cortex, and lPFC (middle and superior PFC). We also found clusters in the precuneus and posterior parietal cortex, which were previously reported to represent the egocentric location (Chadwick et al., 2015). The widely distributed clusters may indicate that the brain regions representing the egocentric target locations can be involved in either generation of the egocentric-target-location information from multiple pieces of information (cognitive map, self-orientation, and target character identity) or its maintenance while preparing for the following response. These distinct functions might be supported by three different large-scale brain networks: the dorsal attention network, frontoparietal control network, and default mode network (Spreng and Schacter., 2011). In contrast to the robust signal observed across different brain networks for egocentric target-location, no cluster was

revealed for allocentric target location relative to the spatial layout of the characters (Fig. 4b, $P < 0.001$, voxel-wise threshold; $P < 0.05$, cluster-corrected), which implies that the target location may be directly retrieved in the form of egocentric coordinates rather than via its allocentric representation.

Increased default-mode network connectivity while locating a target compared with self-locating

The present results showed that the MTL and mPFC signaled a coherent map coding a spatial relationship of the three human characters during the different time periods in which different task demands were required (i.e., self-locating and target-locating). In addition, the MTL and mPFC signaled the different location information even during the same targeting period; MTL areas tended to represent allocentric self-location while the mPFC tended to represent egocentric target location. To investigate how the different functional contributions of the MTL and mPFC were substantiated by whole brain large-scale networks, we conducted a task-based functional connectivity analysis using MTL and mPFC sub-regions as seeds (six and five, respectively). For each seed, the mean regional time course was extracted and correlated with each voxel's time course outside the seed, generating seed-based connectivity maps for each facing and targeting period. Then, we compared the connectivity between the two periods using a permutation test (see Methods for details).

First, the task-based functional connectivity analysis indicated significantly larger connectivity between the MTL and mPFC in the targeting period relative to the facing period ($t(18) = 2.95$, $P = 0.009$). We next examined the connectivity of the MTL and mPFC to the three large-scale brain networks. Both the MTL and mPFC showed significantly larger connectivity to brain areas that belong to the frontoparietal control network during the facing period relative to the targeting period (Fig. 5a, $P < 0.01$, voxel-wise threshold; $P < 0.05$,

cluster-corrected). In contrast, the default mode network and dorsal attention network showed significantly larger connectivity to the MTL and mPFC in the targeting period compared to the facing period (Fig. 5b, $P < 0.01$, voxel-wise threshold; $P < 0.05$, cluster-corrected). These results suggest that both the MTL and mPFC changed their connectivity to the three functional networks across the two task periods. We next evaluated the task-based functional connectivity during each task period based on the three functional network masks (Fig. 5a, b). This ROI analysis revealed that the default mode network was positively correlated with the MTL ($t(18) = 9.42$, $P < 0.001$) and mPFC ($t(18) = 10.63$, $P < 0.001$) for both time periods with a significant increase in the targeting period (Fig. 5c & Fig. S6, top panel; $F(1,72) = 4.63$, $P = 0.03$), regardless of the seeds (MTL or mPFC; $F(1,72) = 0.24$, $P=0.62$). These results suggest that the default mode network contributes more to the retrieval of the target location than the self-location to an external reference during the facing period. In contrast, the frontoparietal control network showed significantly negative connectivity with the MTL ($t(18) = -9.12$, $P < 0.001$) and mPFC ($t(18) = -10.43$, $P < 0.001$) during both task periods, indicating that the frontoparietal control network works competitively with MTL and mPFC areas of the default mode network. This competitive effect was stronger during the targeting period (Fig. 5c & Fig. S6, middle panel; $F(1,72) = 5.82$, $P = 0.02$). Interestingly, despite both the MTL and mPFC being part of the default mode network, they showed opposite connectivity patterns to the dorsal attention network during both periods (Fig. 5c & Fig. S6, bottom panel; $F(1,72) = 46.72$, $P < 0.001$); the MTL positively with the network while the mPFC negatively correlated with it. The connectivity between the MTL and the dorsal attention network increased from the facing to targeting period ($t(18) = 4.31$, $P = 0.0004$). These results demonstrated that the dorsal attention network, which contains the superior parietal lobule (SPL) that represented egocentric target location (Fig. 4a), showed increased coupling with the MTL during the targeting period. On the other hand, the mPFC only

299 attenuated its amplitude of anti-correlated connectivity with the dorsal attention network,
300 which may suggest that egocentric target location represented in the mPFC was not directly
301 transmitted to the dorsal attention network. Considering the increased coupling between the
302 mPFC and default mode network including MTL areas during the targeting period (Fig.
303 5b&c), we hypothesize that the egocentric target location might be transferred from the
304 mPFC to the SPL via the MTL.

Discussion

In this study, we examined neural representations of space defined by three objects and found that both the HPC and mPFC represented the object-based space around the participants. Interestingly, the HPC represented the object-based map when the participants locate their self-body in the environment constructed by the three objects, while the mPFC represented the map when the participants remembered the location of a target object relative to the self-body. These results suggest that the cognitive maps in different brain regions play different functional roles. In addition, during the targeting period, we found different preference in spatial element representation between the MTL and mPFC, more MTL regions reinstated allocentric self-location, while more mPFC regions represented egocentric target location relative to self-location. Increased functional connectivity was observed between the MTL and mPFC under the necessity of the retrieval of the target location from the stored memory (targeting period) compared to when they actually faced the reference object to locate their self-body (facing period). These results suggest that mental representations of the external world formed by the coherent space and its constituent elements may be shared in the default mode network including the MTL and mPFC. The special role of the mPFC in this scheme may be to select the object location based on the mnemonic information including the cognitive map and current self-location on it, which may be propagated from the MTL.

For the detection of "*map*" effect (Fig. 1b), the present task was designed to cancel out effects of a particular encoding experience related with the walking direction as well as a particular object identity that the participants viewed during the facing and targeting periods in each trial by balancing number of trials with each of those confounding factors in each map (see Methods). Therefore, the neural representation of the map information revealed by the RSA cannot be explained by individual perceived information in the present study. Moreover, the participants always stood on the center of the virtual environment during the

facing and targeting periods, during which the map effect was examined. Because of this task design, the map information does not directly indicate self-location information like place fields of place cells in the HPC (O'Keefe and Dostrovsky, 1971). On the other hand, the representations of place-fields are reportedly influenced by the animal's cognitive map, and the existence of cognitive maps could be most clearly demonstrated by a phenomenon known as "remapping", which reportedly occurs in populations of place cells in the rodent HPC (Moser et al., 2017). Therefore, it might be reasonable to interpret the map representations in the left mHPC during the facing period as experimental evidence of "remapping" of place cells in the human HPC even though the participants stood on the same position. However, holding this interpretation predicts that human place cells are localized in the left mHPC. This prediction is against consistent evidence from previous human studies that reported that the right HPC was more involved in encoding and retrieving spatial information than the left HPC (Abrahams et al., 1997; Maguire et al., 1997; Ekstrom et al., 2003; Doeller et al., 2008; Schinazi, 2013). The other possible interpretation for the map representation in the left mHPC is that it may encode an allocentric spatial relationship of the three objects itself. This interpretation is consistent with previous human imaging studies reporting contributions of the left HPC to the imagination of visual scenes, which could be constructed from multiple spatial elements (Addis et al., 2007; Bird et al., 2010). The specific role of the left HPC in relational memory was also reported in non-spatial information domains, including associative learning (Kumaran et al., 2009; Suarez-Jimenez et al., 2018) and social interactions (Tavares et al., 2015;). Taken together, it might be more reasonable to interpret that the clusters in the left mHPC represented a coherent space constructed by the multiple objects rather than its influence on representations of individual spatial elements such as self-location or head direction. RSA also revealed the involvement of the PRC and PHC in MTL signaling the object identity and egocentric view of their spatial layout, respectively, which

might be used for constructing the coherent map from its constituents in the left mHPC. Future studies should address how the coherent map can be constructed by multiple objects in the MTL.

In contrast to the facing period, during the targeting period, the representation of the map information was found in the mPFC but not in the HPC. In addition, the mPFC signaled the egocentric location of a targeting object, while the MTL concurrently signaled the allocentric self-location. Involvement of the mPFC in constructing goal-directed information in the current context is consistent with accumulating evidence showing that the mPFC contributes to decision making or action selection (Saxena et al., 1998; Gallagher et al., 1999; Feierstein, 2006; Spiers and Maguire, 2007; Kable and Glimcher, 2009; Young and Shapiro, 2011; Balaguer et al., 2016; Yamada et al., 2018). These previous studies consistently supported the notion that the mPFC function becomes obvious when an appropriate selection requires mnemonic information in addition to incoming perceptual information (Bradfield, 2015). In this study, together with perceptual information responsible for target object identity, mnemonic information such as the map information and allocentric self-location was required to solve the task. Considering that the MTL could provide all the necessary mnemonic information, a reasonable interpretation is that the mPFC was involved in the selection of one egocentric location among alternative locations rather than the recollection or generation of location information of a target object.

In addition to the HPC and mPFC, the map information has been observed in other brain areas such as the angular gyrus (Seghier, 2013; Price et al., 2016), lateral temporal gyrus (Karnath, 2001; Himmelbach et al., 2006), and precuneus (Cavanna and Trimble, 2006) that also belong to the default mode network. The brain areas in the default mode network, particularly the MTL sub-regions except for the PRC represented allocentric self-location

379 during the targeting period. On the other hand, RSA analysis showed that widely-distributed
380 brain regions were involved in the representation of the egocentric target object location not
381 only in the default mode network but also in the dorsal attention network and frontoparietal
382 control network. The positive and negative functional connectivity between the dorsal
383 attention network and the MTL and mPFC suggest that the egocentric target location signal is
384 transmitted from the mPFC to the brain regions of the dorsal attention network, such as the
385 SPL (Evans et al., 2016), via the MTL, which implies a pivotal functional role of MTL as a
386 hub of mental representation of object signals.

387 Interestingly, the frontoparietal control network showed a strong negative correlation
388 with both the MTL and mPFC during both periods, although the lPFC in the frontoparietal
389 control network represented both the map information and egocentric direction during the
390 targeting period. In addition, the lPFC represented walking direction as well as character
391 identity during both the facing and targeting period. These results suggest that the lPFC
392 computes the target location independently of the default mode network. The parallel
393 contributions of the lPFC and MTL-mPFC in choosing the target location may reflect their
394 different cognitive functions (Jimura et al., 2004). lPFC has long been considered as a center
395 of executive functions (Funahashi, 2017; Miller et al., 2018) equipped with working memory
396 (Andrews et al., 2011; Barbey et al., 2013; Brunoni and Vanderhasselt, 2014; Funahashi,
397 2017). In human fMRI studies, the lPFC has been shown to contribute to the retrieval of task-
398 relevant information from spatial memory when more systematic thinking is required
399 (Epstein et al., 2017; Javadi et al., 2017). In this study, the behavioral task was designed to
400 ensure participants neither actively maintained a spatial configuration of the human
401 characters during the walking period nor any systematic strategy to solve the task, which was
402 confirmed by the post-scanning test results. The greater signal for the cognitive map and the
403 egocentric target location in the mPFC than that in the lPFC may indicate that the current task

404 was easy enough to allow participants to depend only on memory to exhibit top-ceiling
405 performance (Epstein et al., 2017; Javadi et al., 2017).

406 In contrast to previous memory/navigation studies, which examined brain functions
407 using spatial environments consisting of immobile landmarks (e.g., stores) and/or landscapes
408 (e.g., mountains) (Bird et al., 2010; Woollett and Maguire, 2011; Schinazi et al., 2013;
409 Chadwick et al., 2015; Brown et al., 2016), the present study used a spatial environment
410 constructed by only mobile objects that could become targets and references of self-location
411 as well as determine the space (i.e., map) around oneself. This task design allowed us to
412 extract a mental representation of the spatial environment consisting of the minimum
413 essential constituents. This reductionist method could be useful for future studies
414 investigating the construction and functional mechanisms of a cognitive map because of its
415 simplicity. One critical concern might be whether the findings discovered by this reductionist
416 method can be applied to a more complicated cognitive map consisting of large numbers of
417 immobile spatial elements, which could be learned through extensive explorations over a
418 long time period (e.g., the city of London) (Woollett and Maguire, 2011). Another related
419 concern might be whether our brain system holds only one cognitive map or multiple ones at
420 a time (Meister and Buffalo, 2018). For example, we may hold an object-based cognitive map
421 consisting of relevant mobile objects such as same species, predators, and foods, while we
422 may also hold the other cognitive map consisting of landmarks, landscapes and other
423 immobile objects such as trees. Future studies should address the relationships of different
424 types of cognitive maps (e.g., mobile vs immobile, short-term vs. long-term) and their
425 underlying neural mechanisms.

426 The present study discovered neural representations of the space specified by objects
427 around us. This object-based cognitive map seems to interact with representation of self-
428 location in HPC and mediate a selection of egocentric target-location in mPFC, which would

serve for leading us to the goal position. In addition to the spatial navigation, an existence of the object-based cognitive map may equip us with a space representation for persons separately from the background, which may serve for our social interactions (Damasio et al., 1994; Stolk et al., 2015) as well as the encoding and retrieval of episodic memory (Tulving, 2002; Squire and Wixted, 2011).

Supplemental Information

Supplemental Information includes six figures, two tables and two videos. The videos contain trial examples for Day 1 and Day 2. In the video of day 1, please note we only used examples of correct trials in which a green photo border was shown as feedback after response was made. File size: 21.5 MB; Video duration: 1.23 minute; File format: .mp4; Video codec: H.264; Aspect ratio: 1024 x 768.

Author Contributions

B.Z. and Y.N made the experimental design; B.Z. conducted all experiments and data analysis under supervision of Y.N.; B.Z. and Y.N. wrote the paper.

Acknowledgments

The present study was funded by National Natural Science Foundation of China Grant 31421003 (to Y.N.). Computational work was supported by resources provided by the High-performance Computing Platform of Peking University. We thank Li Sheng and Sun Pei for helpful discussions, we also thank Koji Jimura, Rei Akaishi and Cen Yang for comments on an early version of the manuscript.

Main figures

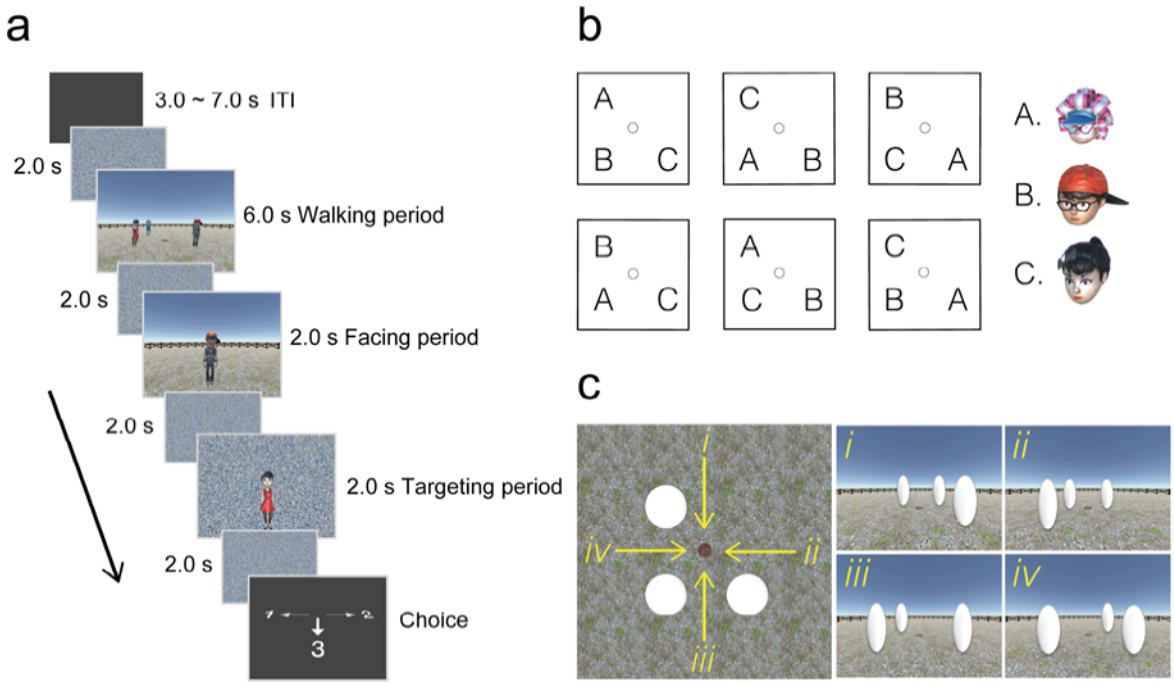

Figure 1: Task design. (a) spatial-memory task. Each trial consisted of three periods. In the walking period, participants walked toward three human characters using the first-person perspective and stopped on a wood plate. In the facing period, one of the human characters was presented, indicating the participant's current self-orientation. In the targeting period, a photo of another character was presented on the scrambled background. The participants chose the direction of the target character relative to their body upon presentation of a response cue. (b) Maps were defined by the relative position of the three human characters, while the unfilled dot represents the wood plate. (c) The walking directions were defined by the spatial layout of the three human characters from the participant's first-person perspective.

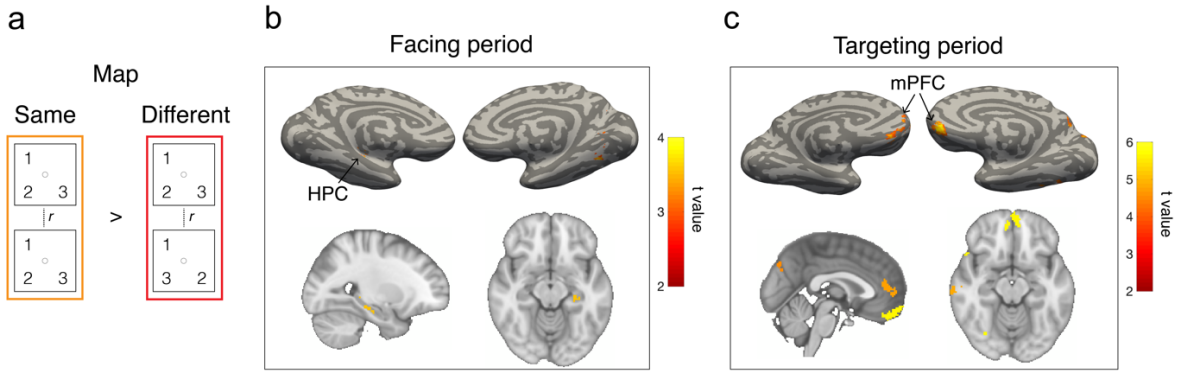

Figure 2: Neural representation of the map information in MTL and mPFC. (a) Schematic representation of decoding the cognitive map using RSA. (b) In the facing period, RSA revealed a cluster in the left middle HPC (mHPC; MNI coordinates: -28,-27,-16; shown on sagittal and transverse section) within the MTL ($P < 0.01$, initial threshold; $P < 0.05$, cluster-corrected; shown on surface). (c) In the targeting period, clusters were revealed in the mPFC but not in the MTL ($P < 0.001$, initial threshold; $P < 0.05$, cluster-corrected). A peak was revealed in the rectus within the mPFC (t value: 5.62; MNI coordinates: 4, 50, -18).

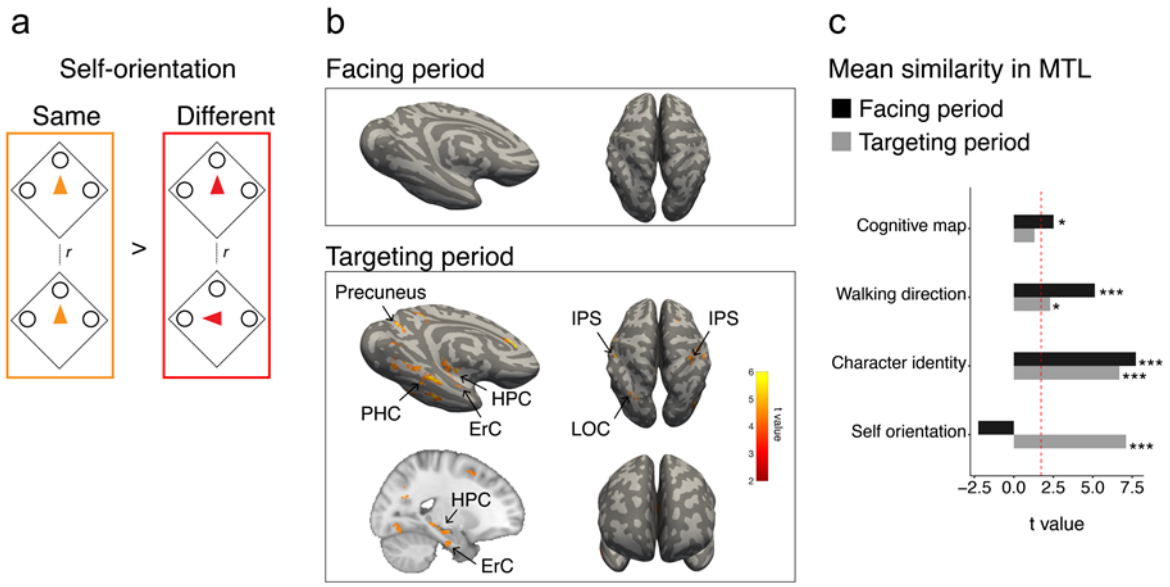

Figure 3: Neural representation of self-orientation on cognitive map. (a) Schematic representation of decoding participants' self-orientation. (b) In the facing period, no cluster was revealed even with the use of a more liberal threshold ($P < 0.01$, initial threshold; $P < 0.05$, cluster-corrected). In the targeting period, clusters were revealed in the MTL (bilateral HPC, PHC, and left ErC) and self-motion areas (inferior parietal cortex, RSC, and lateral occipital cortex). (c) The averaged multi-voxel pattern similarities of the MTL sub-regions (bilateral HPC, PHC and left ErC) based on four spatial parameters. Group level statistics were assessed using the one-tailed t-test. Red dashed line indicates the $p < 0.01$ threshold. * indicates $P < 0.01$, *** indicates $P < 0.001$.

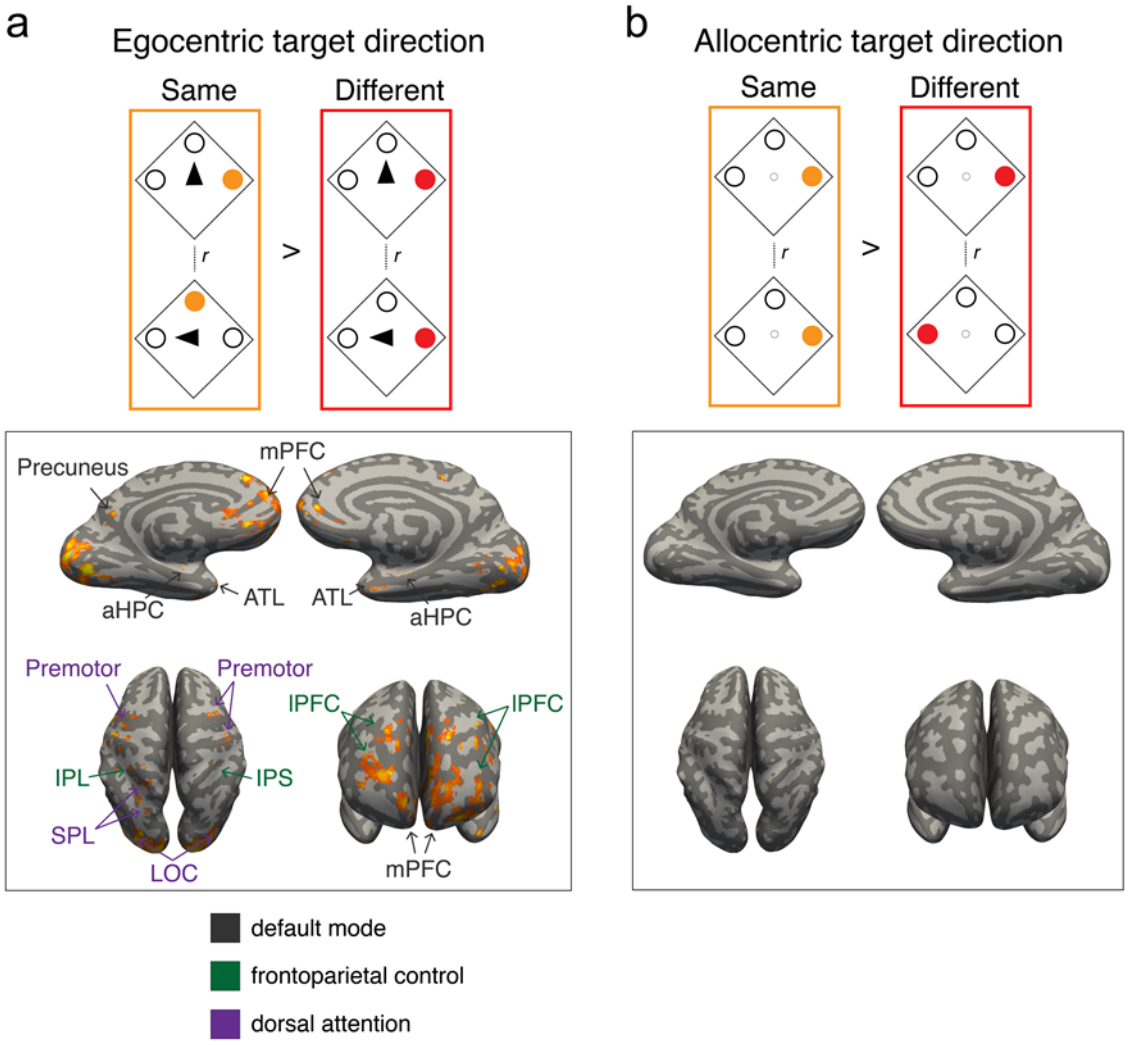

Figure 4: Neural representation of retrieved egocentric target location. (a) Top panel: Schematic representation of decoding the allocentric direction of a target character. Bottom panel: No clusters were revealed even with the use of a liberal threshold ($P < 0.01$, initial threshold; $P < 0.05$, cluster-corrected). (b) Top panel: Schematic representation of decoding the egocentric direction of a target character. Bottom panel: Clusters were revealed across a wide range of brain areas ($P < 0.001$, initial threshold; $P < 0.05$, cluster-corrected). Many of the clusters belonged to one of the following three functional networks: the default mode network, frontoparietal control network, and dorsal attention network.

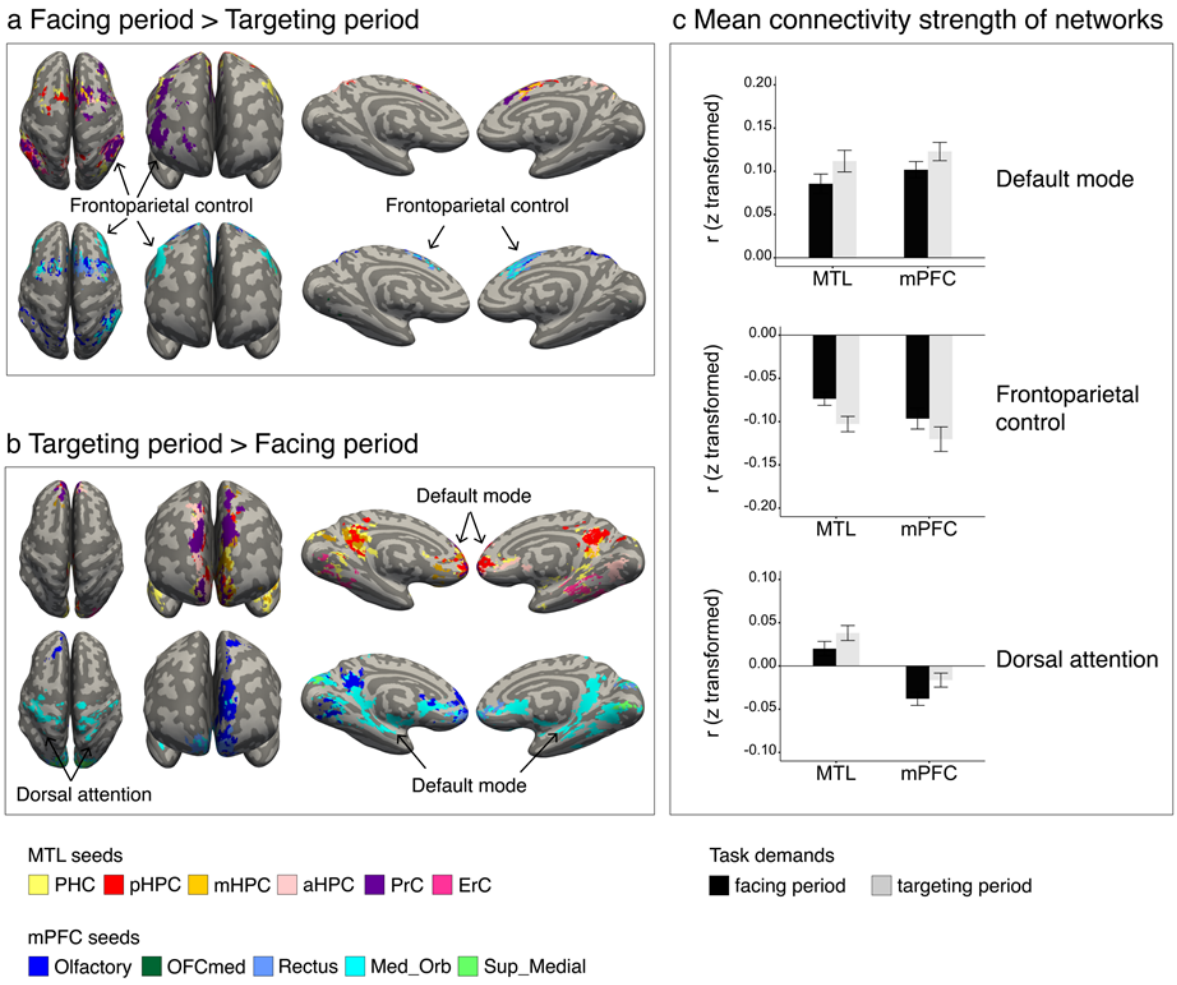

Figure 5: Increased default-mode network connectivity while locating a target compared with locating oneself. Six MTL sub-regions and five mPFC sub-regions were used as anatomical seeds that were highlighted by different colors. All the connectivity brain maps overlapped and were projected on the brain surface. (a) The frontoparietal control network showed enhanced connectivity strength with the MTL and mPFC in the facing period compared to the targeting period ($P < 0.01$, initial threshold; $P < 0.05$, cluster-corrected). (b) The default mode network and dorsal attention network showed enhanced connectivity strength with the MTL and mPFC in the targeting period compared to the facing period ($P < 0.01$, initial threshold; $P < 0.05$, cluster-corrected). (c) The mean connectivity strength of MTL and mPFC sub-regions with three networks, respectively. Note that the two default model network masks were made with the MTL and mPFC excluded, respectively. The masks were used to examine the

503 connectivity between the MTL and mPFC with the remaining areas of the default mode

504 network.

Methods

Participants

Nineteen right-handed university students with normal or corrected-to-normal vision were recruited from Peking University (12 females, 7 males). The average age of the participants was 24.9 years (range: 18–30 years). All participants had no history of psychiatric or neurological disorders and gave their written informed consent prior to the start of the experiment, which was approved by the Research Ethics Committee of Peking University.

Task design

Virtual environment. We programmed a 3D virtual environment using Unity software (Unity Technologies, San Francisco). The environment was designed with a circular fence as a boundary (48 virtual meters in diameter), a flat grassy ground, a uniform blue sky, and with a wood plate surrounded by four vertices of a square placed in the center (Fig. 1b, 4.7 virtual meters for side length). Three human characters (Mixamo, San Francisco, https://www.mixamo.com) were placed on three of the vertices in each trial. A map was defined by the relative relationship of the three human characters (Fig. 1b). From the six possible maps, three of them were pseudo-randomly selected for each participant, and were the only environmental cues relevant to the task requirement, no distal cues were used outside the boundary. Participants performed the task using the first-person perspective with a 90° field of view (aspect ratio = 4:3), they had never seen a top-down view of the virtual environment.

Walking period. Participants walked from one of four starting locations near the circular boundary (4 virtual meters from the boundary) toward the human characters (Fig. 1c) and stopped on the wood plate. The visual stimuli (spatial environment viewed from first-person

perspective) were determined by the combination of the map and walking direction, in other words, each map was presented by four different visual stimuli that were determined by the starting position (Fig. 1c). Importantly, participants were blinded to the map concept throughout the task. The walking period lasted for 6.0 s, during which each character had a 20.6% probability of nodding its head at a random time point between the start and end of walking. There was a 50%, 38.9%, 10.2%, and 0.9% probability for 0, 1, 2, and 3 characters to nod head in each trial; we subjectively selected a 20.6% head-nodding probability for each character to ensure an approximately equal number of trials with head-nodding and no head-nodding. During the walking period, participants were required to pay attention to the heads of the human characters rather than to memorize their spatial arrangement. The height of the participants was 1.8 virtual meters from the ground, which was the same as that of the human characters. No response was required during the walking period.

Two tasks were completed in two consecutive days. On day 1, the participants performed an HND task that did not include spatial-memory trials. On day 2, participants performed a spatial-memory task that included 90% of spatial-memory trials and 10% of HND trials under MRI scanning. Both tasks contain a walking period at the beginning of each trial; therefore, it was impossible to predict the trial-type. Participants were told that remuneration depended only on the performance in the HND trials but were encouraged to perform both trial-types as best as they could (videos of trial examples are available online for both tasks).

Head-nodding detection (HND) task. Participants performed 144 randomly ordered HND trials in a behavioral experimental room. In each trial, a photo of one of the characters was presented on a screen after the walking period, and participants were asked to indicate whether the character nodded its head or not (Fig. S1a). For this task, there was a 50% chance that the character in the presented photo nod head. Feedback was given after the participants

had responded with either green (correct) or red (incorrect) photo border. The stimuli were rendered on a PC and presented on a 27-inch LCD monitor (ViewSonic XG2730) with a screen resolution of 1024 x 768. The HND task was used to examine whether participants paid attention to head-nodding rather than memorizing the spatial arrangement of the characters, which would be indicated by high success rates in the head-nodding test.

Spatial-memory task. During this task, participants performed 144 spatial-memory trials (90%) and 16 HND trials (10%) that lasted ~ 70 min in an MRI scanner. In each trial, participants experienced a "facing period" and a "targeting period" sequentially after the walking period. In the facing period, their self-orientation was changed immediately to one of the human characters (facing-character) without viewpoint transition, and a character with the environment background was presented for 2.0 s with the other two characters being invisible, the participants were instructed to face the character. In the targeting period, a photo of another character (targeting-character) was presented as a target on a scrabbled background for 2.0 s. Each of the three experimental periods was followed by a 2.0-s delay (noise screen). At the end of each trial, participants indicated the direction of the target character relative to their self-body by pressing a button when a cue presented on the screen; no feedback was shown for both trial-types (Fig. 1a). The spatial-memory task contained four experimental sessions, each containing a spatial information combination of 3 maps x 4 walking directions x 3 facing-character identities in each session, with targeting-characters balanced across sessions. After scanning, all participants completed a post-scanning interview and reported the strategy they used to perform the task (Table. S2).

fMRI data acquisition

Imaging data were collected using a 3T Siemens Prisma scanner equipped with a 20-channel receiver head coil. Functional data were acquired with a Multi-band Echo Planer imaging

(EPI) sequence (TR = 2000 ms, TE = 30 ms, matrix size: 112 × 112 x 62, flip angle: 90°, gap = 0 mm; resolution: 2 × 2 × 2.3 mm^3, number of slices: 62, slice thickness: 2 mm, slice orientation: transversal). A high-resolution T1-weighted three-dimensional anatomical data set was collected to aid in registration (MPRAGE, TR = 2530 ms, TE = 2.98 ms, matrix size: 448 x 512 x 192, flip angle: 7°, resolution: 0.5 × 0.5 × 1 mm^3 , number of slices: 192, slice thickness: 1 mm, slice orientation: sagittal). During scanning, experimental stimuli were presented through a Sinorad LCD projector (Shenzhen Sinorad Medical Electronics) onto a 33-inch rear-projection screen located over the subject's head with a resolution of 1024 x 768 and viewed with an angled mirror positioning on the head coil.

fMRI preprocessing

Functional data for each session were preprocessed independently using FSL FEAT (FMRIB's Software Library, version 6.00, https://fsl.fmrib.ox.ac.uk/fsl/fslwiki; Woolrich et al., 2001; Woolrich et al., 2004). For each session, the first three functional volumes were discarded to allow for T1 equilibration, and the remaining functional volumes were slice-time corrected, realigned to the first image, and high-pass filtered at 100 s. For group-level statistics, each session's functional data were registered to a T1-weighted standard image (MNI152) using FSL FLIRT (Jenkinson and Smith, 2001), and this procedure also resampled the functional voxels into a 2 x 2 x 2 mm resolution. For RSA, data were left unsmoothed to preserve any fine-grained spatial information (Chadwick et al., 2012). For functional connectivity analysis, data were smoothed using a 5 mm FWHM Gaussian kernel and were high-pass filtered at 0.01 Hz to remove low-frequency signal drifts.

Anatomical masks

We manually delineated the MTL, including the HPC, PHC, PRC, and ERC on each participant's native space using established protocols (Insausti et al., 1998; Pruessner et al., 2000; Pruessner et al., 2002; Duvernoy, 2005), as well as a delineating software ITK-SNAP (www.itksnap.org). The HPC was further divided into its anterior, middle, and posterior parts using anatomical landmarks of each participant given the anatomical and functional variability along the HPC long axis (Poppenk et al., 2013). For PFC sub-regions, we used the AAL template (Rolls et al., 2015), and selected five mPFC sub-regions for ROI-analysis, which included the rectus, medial orbital gyrus (OFCmed), medial orbital frontal gyrus (Med_Orb), superior medial frontal gyrus (Sup_Med), and olfactory cortex. All ROIs were resampled and aligned with the functional volumes, and voxels outside of the brain were excluded.

Representational similarity analysis (RSA)

Task-relevant information was decoded using RSA. We tried to dissociate the neural effect of facing and targeting period based on 4 s duration from each period onset to the end of following noise period (Zeithamova et al., 2017). First, the trial-based multi-voxel activity patterns of two periods were obtained by creating two separate univariate general linear models (GLM). In each GLM, the 4 s blood-oxygen-level-dependent (BOLD) signals of 36 trials (a session) were modeled using boxcar regressors. In addition to the 36 trial-based regressors of interest, nuisance regressors were included, which included twelve regressors for modeling the visual patterns of the walking period determined by the maps and walking directions, three for modeling the character identities in the remaining period (for example, in the facing period GLM, three targeting characters were specified as nuisance regressors rather than the facing characters), four for modeling head-nodding detection trials, three for modeling 3 directional cues in the response period, and six motion parameters. This

629 procedure generated 36 trial-based multi-voxel patterns in participant's native space (2 x 2 x
630 2.3 mm voxels) for each period, those multi-voxel patterns were normalized prior to
631 subsequent analysis by subtracting the grand mean pattern of the 36 multi-voxel patterns for
632 each session (Vass and Epstein, 2013).

633 Searchlight-based RSA. Next, we computed the representational similarity for each
634 spatial information based on the multi-voxel patterns using a searchlight-based RSA (Libby
635 et al., 2014; Chadwick et al., 2015), which was conducted using custom Matlab (version
636 R2018b, www.mathworks.com/matlab/) scripts. In detail, a sphere with a 6 mm radius was
637 constructed (85 voxels per sphere) for each brain voxel, and the spheres near the edge of the
638 brain with fewer than ten voxels were excluded from the analysis. The activity parameters
639 within each sphere were extracted from each of the 36 multi-voxel patterns, resulting in a 36-
640 column by n-row (number of voxels within the sphere) matrix. The pattern similarity was
641 then calculated between each column-by-column pair using Pearson's correlation, and was
642 normalized using Fisher's r-to-z transformation. This procedure finally generated a 36-by-36
643 correlation matrix for each period in each brain voxel. Next, given that a multi-voxel pattern
644 contains the combination of multiple spatial information, we conducted a GLM for each
645 correlation matrix by specifying multiple categorical regressors to rule out potential
646 influences. Each spatial representation represented specific spatial information and used
647 either indicator "1 (same)" or " 0 (different)" that corresponded with the correlation
648 coefficient of a given column-to-row cell of the correlation matrix. For the facing period, the
649 GLM contained five categorical regressors, which included the (1) "map", (2) "walking
650 direction", and (3) "facing-character identity". Since the participants reported thinking about
651 their bodies rotating between the walking direction and self-orientation relative to the
652 environment, we also added the (4) "rotation angle" (turn left/right 45°, turn left/right 135°),
653 and (5) their "self-orientation" into the GLM. For the targeting period, seven regressors were

built, which included: (1) "map", (2) "walking direction", (3-4) participants' "rotation angle" and "self-orientation", (5) "targeting-character identity", and (6-7) "egocentric and allocentric position of target-character". It is important to note that the "facing-character identity" was not included in the targeting period GLM since the effect of each facing character was regressed out in the GLM computing of multi-voxel activity patterns. r^2 was computed and ranged from 0 to 0.03 for the facing period GLM, and 0 to 0.04 for the targeting period GLM (Table S1). Each regressor's parameter was then assigned to the center voxel of each sphere so that a whole-brain statistical parametric mapping could be generated for each spatial information for each period, with those spatial representations being finally averaged across the four scanner sessions. By using this method, spatial information should be successfully decoded if the regressors stably predict the correlation coefficients in any voxels. A permutation test was used to examine the spatial representation stability across the subjects (Nichols and Holmes, 2002; Winkler et al., 2014).

ROI-based RSA. To validate the spatial representations, we further conducted an independent RSA using anatomical ROIs of MTL and PFC sub-regions. We reasoned that since searchlight analysis identifies the spatial representations as clusters in small portions of anatomical regions, if those representations are stable enough, the corresponding anatomical regions, on average, should show a clear increasing tendency in similarity when spatial information between trial-pairs are similar compared to different such that matching to the searchlight results. To test this, we separated each ROI into the left and right hemispheres and generated 22 anatomical masks (12 for the MTL and 10 for the mPFC). The mPFC masks were normalized into the participants' native space. The RSA procedure for each ROI was similar to searchlight analysis, which produced a 36-by-36 correlation matrix for each period. Next, for each spatial information, the correlation matrix elements were binarized into "same (1)" and "different (0)" conditions. A discrimination score was computed by comparing the

679 difference in the means of two conditions, and thus all matrix elements were used. It is
680 important to note that this procedure is different from the previously reported method where
681 the irrelevant information was controlled. Nevertheless, the aim of our analysis was to
682 maintain an efficient number of samples when computing the correlation mean due to the
683 complex nature of the task. The discrimination scores were averaged across the sessions and
684 were submitted to one-tailed one-sample t-tests against change (zero).
685
686 **Functional connectivity (FC) analysis**
687 To investigate the functional networks for different task demands, we examined the whole-
688 brain FC using each MTL and mPFC sub-region as seed. In detail, based on the preprocessed
689 functional data, we further removed the nuisance covariates by creating a GLM that specified
690 the signal averaged over the lateral ventricles, white matter, and whole brain, six motion
691 parameters, and their derivatives as regressors. The residual signal was bandpass-filtered,
692 leaving signals within the frequency range 0.01 to 0.1 Hz, and was shifted by two TR
693 intervals (4 s) for subsequent analysis (Ranganath et al., 2005; Tompary and Davachi, 2017).
694 Next, for each anatomical mask, a regional time course was computed by extracting and
695 averaging signals over the mask from each facing and targeting period. We then correlated
696 the time course with every voxel in the rest of the brain, resulting in a whole-brain correlation
697 map for each period. The correlation maps were averaged across four scanning sessions and
698 were eventually submitted to a one-tailed t-test for group level statistics.
699
700 **Statistics**
701 The significance of group level statistics was assessed by performing a one-tailed one-sample
702 t-test. For searchlight-based RSA, we used an initial threshold of $p < 0.001$. If no clusters
703 were revealed, a more liberal threshold of $p < 0.01$ was used. For FC analysis, an initial

threshold of $p<0.01$ was used to identify robust network patterns. The reliability of significant effects was examined using a non-parametric statistical inference that does not make assumptions about the distribution of the data, the test was conducted with the FSL randomise package (version v2.9, http://fsl.fmrib.ox.ac.uk/fsl/fslwiki/Randomise)(Winkler et al., 2014) using 5000 random sign-flips and threshold-free clustering. We then reported voxels that were significant at $p < 0.05$ after correcting for multiple comparisons across the entire brain. For other analyses, data distributions were assumed to be normal without formal tests. Analysis of variance (ANOVA) was used to test the difference between experimental conditions; the one-tailed t test was used to test the significance of each anatomical mask in ROI-based RSA.

Reference

Abrahams, S., Pickering, A., Polkey, C. E., & Morris, R. G. (1997). Spatial memory deficits in patients with unilateral damage to the right hippocampal formation. Neuropsychologia, 35(1), 11-24.

Andrews, S. C., Hoy, K. E., Enticott, P. G., Daskalakis, Z. J., & Fitzgerald, P. B. (2011). Improving working memory: the effect of combining cognitive activity and anodal transcranial direct current stimulation to the left dorsolateral prefrontal cortex. Brain stimulation, 4(2), 84-89.

Addis, D. R., Wong, A. T., & Schacter, D. L. (2007). Remembering the past and imagining the future: common and distinct neural substrates during event construction and elaboration. Neuropsychologia, 45(7), 1363-1377.

Barbey, A. K., Koenigs, M., & Grafman, J. (2013). Dorsolateral prefrontal contributions to human working memory. cortex, 49(5), 1195-1205.

Brunoni, A. R., & Vanderhasselt, M. A. (2014). Working memory improvement with non-invasive brain stimulation of the dorsolateral prefrontal cortex: a systematic review and meta-analysis. Brain and cognition, 86, 1-9.

Bird, C. M., Capponi, C., King, J. A., Doeller, C. F., & Burgess, N. (2010). Establishing the boundaries: the hippocampal contribution to imagining scenes. Journal of Neuroscience, 30(35), 11688-11695.

Buffalo, E.A. (2015). Bridging the gap between spatial and mnemonic views of the hippocampal formation. Hippocampus *25*, 713-718.

Balaguer, J., Spiers, H., Hassabis, D., & Summerfield, C. (2016). Neural mechanisms of hierarchical planning in a virtual subway network. Neuron, 90(4), 893-903.

Bradfield, L. A., Dezfouli, A., van Holstein, M., Chieng, B., & Balleine, B. W. (2015). Medial orbitofrontal cortex mediates outcome retrieval in partially observable task situations. Neuron, 88(6), 1268-1280.

Brown, T. I., Carr, V. A., LaRocque, K. F., Favila, S. E., Gordon, A. M., Bowles, B., ... & Wagner, A. D. (2016). Prospective representation of navigational goals in the human hippocampus. Science, 352(6291), 1323-1326.

Cavanna, A.E., and Trimble, M.R. (2006). The precuneus: a review of its functional anatomy and behavioural correlates. Brain : a journal of neurology 129, 564-583.

Campbell, K.L., Madore, K.P., Benoit, R.G., Thakral, P.P., and Schacter, D.L. (2018). Increased hippocampus to ventromedial prefrontal connectivity during the construction of episodic future events. Hippocampus 28, 76-80.

Chadwick, M. J., Jolly, A. E., Amos, D. P., Hassabis, D., & Spiers, H. J. (2015). A goal direction signal in the human entorhinal/subicular region. Current Biology, 25(1), 87-92.

Chadwick, M. J., Bonnici, H. M., & Maguire, E. A. (2012). Decoding information in the human hippocampus: a user's guide. Neuropsychologia, 50(13), 3107-3121.

Duvernoy, H. M. (2005). The human hippocampus: functional anatomy, vascularization and serial sections with MRI. Springer Science & Business Media.

Damasio, H., Grabowski, T., Frank, R., Galaburda, A.M., and Damasio, A.R. (1994). The return of Phineas Gage: clues about the brain from the skull of a famous patient. Science 264, 1102-1105.

Doeller, C. F., King, J. A., & Burgess, N. (2008). Parallel striatal and hippocampal systems for landmarks and boundaries in spatial memory. Proceedings of the National Academy of Sciences, 105(15), 5915-5920.

Ekstrom, A.D., Kahana, M.J., Caplan, J.B., Fields, T.A., Isham, E.A., Newman, E.L., and Fried, I. (2003). Cellular networks underlying human spatial navigation. Nature *425*, 184-188.

Eichenbaum, H. (2017). The role of the hippocampus in navigation is memory. Journal of neurophysiology 117, 1785-1796.

Epstein, R.A., Patai, E.Z., Julian, J.B., and Spiers, H.J. (2017). The cognitive map in humans: spatial navigation and beyond. Nature neuroscience 20, 1504-1513.

Evans, T., Bicanski, A., Bush, D., & Burgess, N. (2016). How environment and self-motion combine in neural representations of space. The Journal of physiology, 594(22), 6535-6546.

Feierstein, C. E., Quirk, M. C., Uchida, N., Sosulski, D. L., & Mainen, Z. F. (2006). Representation of spatial goals in rat orbitofrontal cortex. Neuron, 51(4), 495-507.

Funahashi, S. (2017). Prefrontal Contribution to Decision-Making under Free-Choice Conditions. Frontiers in neuroscience 11, 431.

Gaesser, B., Spreng, R. N., McLelland, V. C., Addis, D. R., & Schacter, D. L. (2013). Imagining the future: evidence for a hippocampal contribution to constructive processing. Hippocampus, 23(12), 1150-1161.

Gallagher, M., McMahan, R. W., & Schoenbaum, G. (1999). Orbitofrontal cortex and representation of incentive value in associative learning. Journal of Neuroscience, 19(15), 6610-6614.

Himmelbach, M., Erb, M., and Karnath, H.O. (2006). Exploring the visual world: the neural substrate of spatial orienting. NeuroImage 32, 1747-1759.

Hargreaves, E.L., Rao, G., Lee, I., and Knierim, J.J. (2005). Major dissociation between medial and lateral entorhinal input to dorsal hippocampus. Science 308, 1792-1794.

Hassabis, D., & Maguire, E. A. (2007). Deconstructing episodic memory with construction. Trends in cognitive sciences, 11(7), 299-306.

814 Insausti, R., Juottonen, K., Soininen, H., Insausti, A. M., Partanen, K., Vainio, P., ... &
815 Pitkänen, A. (1998). MR volumetric analysis of the human entorhinal, perirhinal, and
816 temporopolar cortices. American Journal of Neuroradiology, 19(4), 659-671.
817

818 Javadi, A.H., Emo, B., Howard, L.R., Zisch, F.E., Yu, Y., Knight, R., Pinelo Silva, J., and
819 Spiers, H.J. (2017). Hippocampal and prefrontal processing of network topology to simulate
820 the future. Nature communications 8, 14652.
821
822 Jenkinson, M., & Smith, S. (2001). A global optimisation method for robust affine
823 registration of brain images. Medical image analysis, 5(2), 143-156.
824
825 Jimura, K., Konishi, S., and Miyashita, Y. (2004). Dissociable concurrent activity of lateral
826 and medial frontal lobe during negative feedback processing. NeuroImage *22*, 1578-1586.
827
828 Karnath, H. O. (2001). New insights into the functions of the superior temporal
829 cortex. Nature Reviews Neuroscience, 2(8), 568.
830
831 Kumaran, D., Summerfield, J. J., Hassabis, D., & Maguire, E. A. (2009). Tracking the
832 emergence of conceptual knowledge during human decision making. Neuron, 63(6), 889-901.
833
834 Kriegeskorte, N., Goebel, R., & Bandettini, P. (2006). Information-based functional brain
835 mapping. Proceedings of the National Academy of Sciences, 103(10), 3863-3868.
836
837 Kriegeskorte, N., Mur, M., Ruff, D. A., Kiani, R., Bodurka, J., Esteky, H., ... & Bandettini, P.
838 A. (2008). Matching categorical object representations in inferior temporal cortex of man and
839 monkey. Neuron, 60(6), 1126-1141.
840
841 Kable, J.W., and Glimcher, P.W. (2009). The neurobiology of decision: consensus and
842 controversy. Neuron *63*, 733-745.
843
844 Konishi, S., Wheeler, M.E., Donaldson, D.I., and Buckner, R.L. (2000). Neural correlates of
845 episodic retrieval success. NeuroImage *12*, 276-286.
846
847 Libby, L. A., Hannula, D. E., & Ranganath, C. (2014). Medial temporal lobe coding of item
848 and spatial information during relational binding in working memory. Journal of
849 Neuroscience, 34(43), 14233-14242.
850
851 Meister, M.L.R., and Buffalo, E.A. (2018). Neurons in primate entorhinal cortex represent
852 gaze position in multiple spatial reference frames. The Journal of neuroscience : the official
853 journal of the Society for Neuroscience.
854
855 Miller, E. K., Lundqvist, M., & Bastos, A. M. (2018). Working Memory 2.0. Neuron, 100(2),
856 463-475.
857
858 Moser, E.I., Moser, M.B., and McNaughton, B.L. (2017). Spatial representation in the
859 hippocampal formation: a history. Nature neuroscience 20, 1448-1464.
860

Maguire, E. A., Frackowiak, R. S., & Frith, C. D. (1997). Recalling routes around London: activation of the right hippocampus in taxi drivers. Journal of neuroscience, 17(18), 7103-7110.

McCormick, C., Ciaramelli, E., De Luca, F., and Maguire, E.A. (2018). Comparing and Contrasting the Cognitive Effects of Hippocampal and Ventromedial Prefrontal Cortex Damage: A Review of Human Lesion Studies. Neuroscience 374, 295-318.

Nakazawa, K., Quirk, M.C., Chitwood, R.A., Watanabe, M., Yeckel, M.F., Sun, L.D., Kato, A., Carr, C.A., Johnston, D., Wilson, M.A., et al. (2002). Requirement for hippocampal CA3 NMDA receptors in associative memory recall. Science 297, 211-218.

Nichols, T. E., & Holmes, A. P. (2002). Nonparametric permutation tests for functional neuroimaging: a primer with examples. Human brain mapping, 15(1), 1-25.

Naya, Y., and Suzuki, W.A. (2011). Integrating what and when across the primate medial temporal lobe. Science 333, 773-776.

Naya, Y., Yoshida, M., and Miyashita, Y. (2001). Backward spreading of memory-retrieval signal in the primate temporal cortex. Science *291*, 661-664.

O'Keefe, J., & Dostrovsky, J. (1971). The hippocampus as a spatial map: preliminary evidence from unit activity in the freely-moving rat. Brain research.

Pruessner, J. C., Li, L. M., Serles, W., Pruessner, M., Collins, D. L., Kabani, N., ... & Evans, A. C. (2000). Volumetry of hippocampus and amygdala with high-resolution MRI and three-dimensional analysis software: minimizing the discrepancies between laboratories. Cerebral cortex, 10(4), 433-442.

Pruessner, J. C., Köhler, S., Crane, J., Pruessner, M., Lord, C., Byrne, A., ... & Evans, A. C. (2002). Volumetry of temporopolar, perirhinal, entorhinal and parahippocampal cortex from high-resolution MR images: considering the variability of the collateral sulcus. Cerebral Cortex, 12(12), 1342-1353.

Packard, M.G., and McGaugh, J.L. (1996). Inactivation of hippocampus or caudate nucleus with lidocaine differentially affects expression of place and response learning. Neurobiology of learning and memory 65, 65-72.

Poppenk, J., Evensmoen, H. R., Moscovitch, M., & Nadel, L. (2013). Long-axis specialization of the human hippocampus. Trends in cognitive sciences, 17(5), 230-240.

Price, A. R., Peelle, J. E., Bonner, M. F., Grossman, M., & Hamilton, R. H. (2016). Causal evidence for a mechanism of semantic integration in the angular gyrus as revealed by high-definition transcranial direct current stimulation. Journal of Neuroscience, 36(13), 3829-3838.

Ranganath, C., & Ritchey, M. (2012). Two cortical systems for memory-guided behaviour. Nature Reviews Neuroscience, 13(10), 713.

Ranganath, C., Heller, A., Cohen, M. X., Brozinsky, C. J., & Rissman, J. (2005). Functional connectivity with the hippocampus during successful memory formation. Hippocampus, 15(8), 997-1005.

Rolls, E. T., Joliot, M., & Tzourio-Mazoyer, N. (2015). Implementation of a new parcellation of the orbitofrontal cortex in the automated anatomical labeling atlas. Neuroimage, 122, 1-5.

Redish, A.D., and Touretzky, D.S. (1998). The role of the hippocampus in solving the Morris water maze. Neural computation 10, 73-111.

Seghier, M. L. (2013). The angular gyrus: multiple functions and multiple subdivisions. The Neuroscientist, 19(1), 43-61.

Suarez-Jimenez, B., Bisby, J. A., Horner, A. J., King, J. A., Pine, D. S., & Burgess, N. (2018). Linked networks for learning and expressing location-specific threat. Proceedings of the National Academy of Sciences, 115(5), E1032-E1040.

Spiers, H. J., & Maguire, E. A. (2007). A navigational guidance system in the human brain. Hippocampus, 17(8), 618-626.

Schinazi, V. R., Nardi, D., Newcombe, N. S., Shipley, T. F., & Epstein, R. A. (2013). Hippocampal size predicts rapid learning of a cognitive map in humans. Hippocampus, 23(6), 515-528.

Squire, L.R., and Wixted, J.T. (2011). The cognitive neuroscience of human memory since H.M. Annual review of neuroscience 34, 259-288.

Schacter, D.L., Addis, D.R., and Buckner, R.L. (2007). Remembering the past to imagine the future: the prospective brain. Nature reviews Neuroscience 8, 657-661.

Spreng, R. N., & Schacter, D. L. (2011). Default network modulation and large-scale network interactivity in healthy young and old adults. Cerebral Cortex, 22(11), 2610-2621.

Schacter, D.L. (2012). Adaptive constructive processes and the future of memory. The American psychologist 67, 603-613.

Stolk, A., D'Imperio, D., di Pellegrino, G., and Toni, I. (2015). Altered communicative decisions following ventromedial prefrontal lesions. Current biology : CB 25, 1469-1474.

Saxena, S., Brody, A. L., Schwartz, J. M., & Baxter, L. R. (1998). Neuroimaging and frontal-subcortical circuitry in obsessive-compulsive disorder. The British Journal of Psychiatry, 173(S35), 26-37.

Suzuki, W., and Naya, Y. (2011). Two routes for remembering the past. Cell *147*, 493-495.

Suzuki, W.A., and Naya, Y. (2014). The perirhinal cortex. Annual review of neuroscience *37*, 39-53.

Tolman, E. C. (1948). Cognitive maps in rats and men. Psychological review, 55(4), 189.

960 Tavares, R. M., Mendelsohn, A., Grossman, Y., Williams, C. H., Shapiro, M., Trope, Y., &
961 Schiller, D. (2015). A map for social navigation in the human brain. Neuron, 87(1), 231-243.
962
963 Tulving, E. (2002). Episodic memory: from mind to brain. Annual review of
964 psychology, 53(1), 1-25.
965
966 Tompary, A., & Davachi, L. (2017). Consolidation promotes the emergence of
967 representational overlap in the hippocampus and medial prefrontal cortex. Neuron, 96(1),
968 228-241.
969
970 Vass LK, Epstein RA (2013) Abstract representations of location and facing direction in the
971 human brain. J Neurosci 33:6133–6142. CrossRef Medline
972
973 Woollett, K., & Maguire, E. A. (2011). Acquiring "the Knowledge" of London's layout
974 drives structural brain changes. Current biology, 21(24), 2109-2114.
975
976 Winkler, A. M., Ridgway, G. R., Webster, M. A., Smith, S. M., & Nichols, T. E. (2014).
977 Permutation inference for the general linear model. Neuroimage, 92, 381-397.
978
979 Wang, C., Chen, X., Lee, H., Deshmukh, S.S., Yoganarasimha, D., Savelli, F., and Knierim,
980 J.J. (2018). Egocentric coding of external items in the lateral entorhinal cortex. Science 362,
981 945-949.
982
983 Woolrich, M. W., Ripley, B. D., Brady, M., & Smith, S. M. (2001). Temporal
984 Autocorrelation in Univariate Linear Modeling of FMRI Data. NeuroImage, 14(6), 1370–
985 1386.
986
987 Woolrich, M. W., Behrens, T. E. J., & Smith, S. M. (2004). Constrained linear basis sets for
988 HRF modelling using Variational Bayes. NeuroImage, 21(4), 1748–1761.
989
990 Wikenheiser, A. M., & Schoenbaum, G. (2016). Over the river, through the woods: cognitive
991 maps in the hippocampus and orbitofrontal cortex. Nature Reviews Neuroscience, 17(8), 513.
992
993 Young, J. J., & Shapiro, M. L. (2011). Dynamic coding of goal-directed paths by orbital
994 prefrontal cortex. Journal of Neuroscience, 31(16), 5989-6000.
995
996 Yamada, H., Louie, K., Tymula, A., and Glimcher, P.W. (2018). Free choice shapes
997 normalized value signals in medial orbitofrontal cortex. Nature communications *9*, 162.
998
999 Zeithamova, D., de Araujo Sanchez, M. A., & Adke, A. (2017). Trial timing and pattern-
1000 information analyses of fMRI data. Neuroimage, 153, 221-231.
1001